





Investigation of neutron emission through the local odd-even effect as a function of the fission product kinetic energy

S. Julien-Laferrière,^{1,2} A. Chebboubi ^{1,*} G. Kessedjian,² O. Serot,¹ O. Litaize ¹ A. Blanc,³
U. Köster ³ O. Méplan,² M. Ramdhane ² and C. Sage²

¹CEA, DES, IRESNE, DER, SPRC, Physics Studies Laboratory, Cadarache, F-13108 Saint-Paul-lès-Durance, France

²LPSC, Université Grenoble-Alpes, CNRS/IN2P3, F-38026 Grenoble Cedex, France

³Institut Laue-Langevin, F-38042 Grenoble Cedex 9, France



(Received 20 December 2019; revised 6 April 2020; accepted 29 July 2020; published 3 September 2020)

A recent experimental campaign was completed at the LOHENGRIN spectrometer. It was dedicated to the determination of the local odd-even effect as a function of the fission product kinetic energy for a given mass. We discuss here the mass $A = 139$ produced from the thermal neutron induced fission of ^{241}Pu . A comparison with the Monte Carlo code FIFRELIN allows one to interpret these data in regards to the neutron emission process. The long term goal is to test and validate the phenomenological temperature ratio law used in FIFRELIN to split the total excitation energy between both fission fragments.

DOI: [10.1103/PhysRevC.102.034602](https://doi.org/10.1103/PhysRevC.102.034602)

I. INTRODUCTION

Studies of new and current nuclear reactors rely increasingly on numerical tools. Because of the increase in computational power and the improvement of neutron transport codes, limits on precision are now shifting towards inputs derived from evaluated nuclear data. These evaluated data are a combination of experimental and theoretical knowledge. One way to improve such evaluated data is to perform more accurate measurements and develop more physical models. In this framework, the nuclear fission process [1,2] continues to challenge physicists despite being discovered 80 years ago. Plenty of models are available with different fundamental hypotheses to explain nuclear fission [3–10]. Several experimental fission observables have been studied such as mass and isotopic yields. Among these fission observables, an investigation of the local proton odd-even effect (after neutron emission) $\delta_Z(A)$ can be performed:

$$\delta_Z(A) = \frac{\sum_e Y(A, Z_e) - \sum_o Y(A, Z_o)}{Y(A)} \quad (1)$$

where indices e and o correspond to even and odd parities respectively. The mass and isotopic yields (after neutron emission) are referred as $Y(A)$ and $Y(A, Z)$ respectively.

Moreover the dependence of $\delta_Z(A)$ on fission product kinetic energy could be used to deduce the total excitation energy sharing at scission between both fission fragments. Determination of the excitation energy repartition is essential in the calculation of the prompt neutron and gamma spectra. This observable is complementary to the isomeric ratio measurements as a function of the fission product kinetic energy [11].

In the past, the global proton odd-even effect δ_Z was investigated as a function of the fission product kinetic energy [12–14]. It showed that δ_Z increases with the fission product kinetic energy for the three reactions investigated [$^{232}\text{U}(n_{th}, f)$, $^{233}\text{U}(n_{th}, f)$, $^{229}\text{Th}(n_{th}, f)$].

In this article, we first introduce a new methodology for data taking and analysis of isotopic yield measurements with the LOHENGRIN spectrometer. It will be illustrated with the mass $A = 139$. Then, we report the measurement of the local odd-even effect as a function of the fission product kinetic energy for the mass $A = 139$ in the thermal neutron induced fission of ^{241}Pu .

II. EXPERIMENTAL SETUP

The $\delta_Z(A)$ measurement was carried out using the LOHENGRIN recoil separator for fission products [15] located at the high-flux reactor of Institut Laue-Langevin (ILL) in Grenoble, France. The fission target was placed in a beam tube under a neutron flux of about $5 \times 10^{14} \text{ n cm}^{-2} \text{ s}^{-1}$. In order to reduce the target self-sputtering and improve its burn-up behavior control [16], the target is covered by a thin nickel foil ($\approx 0.25 \mu\text{m}$).

The emerging ionized fission products are first deflected by an horizontal magnetic field and then by a vertical electrostatic field. Note that the spectrometer operates under secondary vacuum ($\approx 10^{-6}$ mbar). Fission products with the same mass over ionic charge $\frac{A}{q}$ and kinetic energy over ionic charge $\frac{E_k}{q}$ ratios have the same trajectory. Finally, the last part of the LOHENGRIN spectrometer is a focusing magnet [17] that can be switched on or (switched) off. It allows us to reach two experimental positions to disentangle the selected triplets (A, q, E_k) . The “straight” position enables one to measure the mass yields by using a double anode Frisch grid ionization chamber (IC) as a detector. The “curved” position takes

* abdelhazize.chebboubi@cea.fr

advantage of the second magnetic field to increase particle density at the focal plane position. In other words, it refocuses ions with different kinetic energies and deflects them towards an array of detectors. In this case, fission products end up on a movable tape (inside a vacuum chamber) surrounded by two clovers. Each clover contains four high purity germanium (HPGe) detectors. It is designed to calculate the isotopic yields by measuring the characteristic γ -ray energy for each isotope decay. Shown results mainly come from the “curved” position setup. Note that all quantities used in the following (kinetic energy, mass, etc.) correspond to post neutron emission quantities unless otherwise specified.

III. DATA TAKING AND ANALYSIS

The local odd-even effect depends directly on the isotopic and mass yields. In this section, descriptions of mass and isotopic yield measurements are shown. More details can be found in Refs. [18–21].

A. Mass yield

As previously explained, the LOHENGRIN spectrometer selects triplets (A, E_k, q) . To detect the mass of the incoming ions, an IC is used at the “straight” position to measure the kinetic energy and therefore the associated mass. The number of counts $N(A, q, E_k \pm \frac{\Delta E_k}{2}, \Delta t_m, t)$ extracted from the IC depends on the mass A , the ionic charge q , the kinetic energy E_k , the LOHENGRIN energy resolution ΔE_k , the measurement time Δt_m , and the time t since the beginning of the experiment. Indeed since the target is under harsh conditions [16], the fissile material significantly evolves with time. Measurements of the ionic charge distribution and kinetic energy distribution of the same mass ($A = 136$) are regularly done throughout the whole experimental period in order to take into account this effect. This observable is called burn-up (BU). Finally, the relative mass yield $\mathcal{N}(A)$ is written

$$\mathcal{N}(A) = \sum_{E_k} \sum_q \frac{N(A, q, E_k, \Delta t_m, t)}{\text{BU}(t) \times \Delta t_m \times E_k}, \quad (2)$$

where the division by E_k accounts for the energy acceptance ΔE_k which is proportional to E_k . Because of the limited beam time, it is impossible to thoroughly measure all E_k and q . Moreover, it has been shown that a correlation exists between E_k and q [18–20,22,23]. To take into account this effect, at least three measurements of the kinetic energy distribution are done at three different ionic charges $q_{i=1,\dots,3}$. Then, two linear fits are performed: one of the mean kinetic energy $\overline{E_k}$ as a function of the ionic charge and one of the standard deviation σ_{E_k} as a function of the ionic charge. Therefore, three estimations of the relative mass yield $\mathcal{N}(A, q_i)$ are computed. An additional ionic charge distribution measurement is performed, for a fixed kinetic energy E_k^\times . This measurement allows one to weight each kinetic energy distribution by the probability of production of the given ionic charge $P(q_i)$. Note that this distribution is corrected from the correlation between

E_k and q as explained previously. Finally, Eq. (2) becomes

$$\mathcal{N}(A, q_i) = \frac{1}{P(q_i)} \sum_{E_k} \frac{N(A, q_i, E_k, \Delta t_m, t)}{\text{BU}(t) \times \Delta t_m \times E_k},$$

$$P(q) \propto N(A, q, E_k^\times, \Delta t_m, t) \exp\left(-\frac{(\overline{E_k}(q) - E_k^\times)^2}{2\sigma_{E_k}^2(q)}\right),$$

$$\sum_q P(q) = 1. \quad (3)$$

These relative mass yields are then combined to have one final estimation of the mass yield $\overline{\mathcal{N}}(A)$ by taking into account the covariance matrix $C_{ij} = \text{Cov}(\mathcal{N}(A, q_i), \mathcal{N}(A, q_j))$. The dependences between the $\mathcal{N}(A, q_i)$ are held by $P(q)$ and $\text{BU}(t)$. Therefore, $P(q)$ and $\text{BU}(t)$ are used to build this covariance matrix as detailed in Refs [20,21]. $\overline{\mathcal{N}}(A)$ is written

$$\overline{\mathcal{N}}(A) = \left(\sum_{i,j} C_{ij}^{-1} \right)^{-1} \left(\sum_{i,j} C_{ij}^{-1} \mathcal{N}(A, q_j) \right). \quad (4)$$

Then a χ^2 test is performed with a confidence level of 90%. If it is unsuccessful, then an additional independent uncertainty is added to the diagonal elements of the covariance matrix C [20]. This additional uncertainty reflects the dispersion of the measurements and the limits of the procedure explained above. At the end, the absolute mass yield is

$$Y(A) = 2 \times \frac{\overline{\mathcal{N}}(A)}{\sum_A \overline{\mathcal{N}}(A)}. \quad (5)$$

However, it is difficult to measure all masses on the LOHENGRIN facility. Nevertheless, the collaboration aim is to provide absolute mass yields independently from nuclear databases. Therefore, at least 99.5% of a mass yield peak (heavy or light) is measured. The induced bias is taken into account in the final uncertainty for all measured masses. It should be noted that several campaigns are required to obtain enough experimental data. At least ten masses are common between each campaign. A cross normalization between each campaign is performed using these masses.

Here is a synthesis of how measurements and associated analysis of the mass yields are performed on the LOHENGRIN recoil spectrometer:

- (1) Measurements of at least three kinetic energy distributions for different ionic charges q_i and one ionic charge distribution at E_k^\times with the IC.
- (2) Computation of the correlation between E_k and q through linear fits of $\overline{E_k}(q)$ and $\sigma_{E_k}(q)$.
- (3) Computation of the relative mass yield for each kinetic energy distribution $\mathcal{N}(A, q_i)$ using Eq. (3).
- (4) Computation of the average relative mass yield $\overline{\mathcal{N}}(A)$ using Eq. (4).
- (5) Computation of the absolute mass yield using Eq. (5).

B. Isotopic yield

Assessment of nuclear charge of fission products is performed through the measurement of the associated β^- delayed γ emission. To detect these γ rays, two clovers are used at

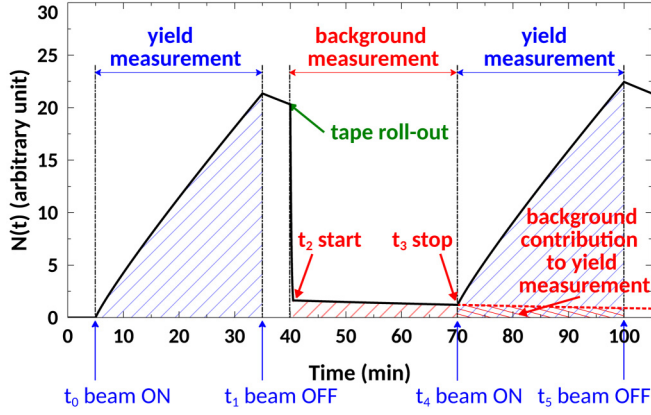


FIG. 1. Scheme of the isotopic evolution $N(t)$ over time. The full lines correspond to the deposited isotopes on the tape and on the vacuum chamber. When the tape is moved and the LOHENGRIN setting is changed, a background can be detected and must be subtracted. This background is coming from ions implanted into the window support grid and ions scattered to the vacuum chamber edges.

the “curved” position. Each clover is made of four HPGe detectors and surrounds a vacuum chamber with a movable tape inside. The beam associated to a specific triplet selection (A, q, E_k) is implanted on the movable tape. During the implantation (beam ON), the associated γ rays are recorded during a time range $\Delta t_m = 20\text{--}30$ minutes. Then, the tape is moved to remove the remaining radioactivity (beam OFF). A new measurement (beam OFF) of $\Delta t_m = 20\text{--}30$ minutes is started in order to estimate the background coming from the vacuum chamber. Indeed the beam is not perfectly collimated. Therefore, certain amount of ions are implanted on the vacuum chamber instead of the movable tape. After measuring the background, the LOHENGRIN setting is changed to a new triplet selection (A', q', E'_k) and a new collection is started (beam ON). Figure 1 sums up the method.

For a given mass, only the ionic charge distribution is measured with the γ detectors at a given kinetic energy E_k^\times , because of the limited beam time. The number of decays N_d of an isotope is written

$$N_{d_\gamma}(A, Z, q, E_k^\times, \Delta t_m, t) = \frac{N_\gamma(A, Z, q, E_k^\times, \Delta t_m, t)}{\epsilon_\gamma I_\gamma f_\gamma}. \quad (6)$$

The number of counts N_γ of a given γ transition is extracted using program Tv [24]. The efficiency ϵ_γ is extracted from a Monte Carlo simulation of the experimental setup. Then, it is validated using experimental data from point sources (^{60}Co , ^{133}Ba , ^{207}Bi) and online beam isotopes (^{96}Y , ^{134}Te), both covering the range 100 keV – 2.3 MeV. The intensity I_γ has been taken from a nuclear database [25]. I_γ is the product of a relative factor I_γ^{rel} and a normalization factor I_{norm}^γ : $I_\gamma = I_\gamma^{\text{rel}} I_{\text{norm}}^\gamma$. Finally, the sum effect correction factor f_γ is calculated with the TRUECOINC software [26]. This factor reflects the misestimation of the detected γ transition. Sometimes two successive γ rays (E_{γ_1} , E_{γ_2}) of the same cascade can be detected simultaneously as one γ transition

($E_\gamma = E_{\gamma_1} + E_{\gamma_2}$). At this step, the different γ rays are used to estimate an average number of decays, \bar{N}_d :

$$\begin{aligned} \bar{N}_d(A, Z, q, E_k^\times, \Delta t_m, t) \\ = \left(\sum_{i,j} C_{ij}^{-1} \right)^{-1} \left(\sum_{i,j} C_{ij}^{-1} N_{d_{\gamma_j}}(A, Z, q, E_k^\times, \Delta t_m, t) \right) \end{aligned} \quad (7)$$

with $C_{ij} = \text{Cov}(N_{d_{\gamma_i}}, N_{d_{\gamma_j}})$. Details on the building of this matrix can be found in Ref. [20]. Similarly to the mass yield case, if the χ^2 test with a confidence level of 90% is unsuccessful, an additional uncertainty is taken into account. Only contributions coming from fission (and not from the deposited background) are of interest. Assessment of the number of decays coming from the contamination of the vacuum chamber $N_{d_{\text{cont}}}$ is detailed in the last section of Appendix A. Therefore the corrected number of decays coming from the nuclear fission process N_{d_f} is written

$$\begin{aligned} \bar{N}_{d_f}(A, Z, q, E_k^\times, \Delta t_m, t) \\ = \bar{N}_d(A, Z, q, E_k^\times, \Delta t_m, t) \\ - \bar{N}_{d_{\text{cont}}}(A, Z, q, E_k^\times, \Delta t_m, t). \end{aligned} \quad (8)$$

The next step is to compute the fission rate τ by resolving the matrix form of the Bateman equations:

$$\boldsymbol{\tau}(A, q, E_k^\times, t) = \mathbf{B} \mathbf{N}_{d_f}(A, q, E_k^\times, \Delta t_m, t) \quad (9)$$

with $\boldsymbol{\tau}(A, q, E_k^\times, t)$ the vector of $\tau(A, Z, q, E_k^\times, t)$ and $\mathbf{N}_{d_f}(A, q, E_k^\times, \Delta t_m, t)$ the vector of $N_{d_f}(A, Z, q, E_k^\times, \Delta t_m, t)$. \mathbf{B} [from Eq. (A11)] values depend on the branching ratios (from one isotope to another), the decay probability λ of each isotope of the isobaric chain, and the acquisition time Δt_m . See Appendix for more details on corrections involving Bateman equations.

Then, the fission rate is corrected by the probability of production of the given kinetic energy $P(E_k^\times)$ to assess the relative isotopic yield $\mathcal{N}(A, Z)$. However, this probability also depends on the ionic charge as previously explained. Therefore, this probability is expressed as

$$\begin{aligned} P(E_k^\times) &= \int_{E_k^\times - \frac{\Delta E_k^\times}{2}}^{E_k^\times + \frac{\Delta E_k^\times}{2}} \rho(E_k) dE_k, \\ \rho(E_k) &= \frac{1}{\sqrt{2\pi} \sigma_{E_k}(q)} \exp\left(-\frac{[E_k - \bar{E}_k(q)]^2}{2\sigma_{E_k}(q)^2}\right). \end{aligned} \quad (10)$$

Quantities $\bar{E}_k(q)$ and $\sigma_{E_k}(q)$ are derived from the measurements of the (at least) three different kinetic energy distributions obtained with the IC. A linear evolution is expected for both quantities. This approach implies two approximations. First a Gaussian form of the kinetic energy distribution is supposed. Second, the probability $P(E_k)$ is supposed to be independent of the isotope. Indeed, the kinetic energy distribution measured with the IC is related to the mass (here

$A = 139$) and not the isotope. $\mathcal{N}(A, Z)$ is then written

$$\mathcal{N}(A, Z) = \sum_q \frac{\tau(A, Z, q, E_k^\times, t)}{\text{BU}(t) \times P(E_k^\times)}. \quad (11)$$

The absolute normalization is achieved in two steps. First, the isobaric chain $A = 139$ is considered as a reference. Indeed, four isotopes, ^{139}I , ^{139}Xe , ^{139}Cs , and ^{139}Ba , are detected for this chain. The independent yield sum of these four isotopes corresponds approximately to 99.5% of the mass yield according to the nuclear data libraries [27,28]. The bias from the nonobserved 0.5% is taken into account in the final uncertainty similarly to the mass yield absolute normalization. This latter is negligible by comparison with the other sources of uncertainties. Then it can be written

$$Y(A = 139) = k_{139} \sum_Z \mathcal{N}(A = 139, Z). \quad (12)$$

Finally, the absolute isotopic yields can be written for all masses and isotopes:

$$Y(A, Z) = k_{139} \times \mathcal{N}(A, Z). \quad (13)$$

However, this solution is not optimal since the absolute isotopic yields of all the measured masses are dependent on the ones from mass 139. Unfortunately, this is the only solution to get absolute isotopic yields since not all nuclei for a given mass are detected (except for $A = 139$).

Below is a synthesis of how measurements and associated analysis of the isotopic yields are performed on the LOHEN-GRIN recoil spectrometer:

- (1) Carrying out the same procedure as for the mass yield case.
- (2) Measurement of the ionic charge distribution with HPGe clovers by implanting ions on a movable tape. Between each ionic charge measurement, a background measurement is performed (see Fig. 1).
- (3) Extraction of the number of counts for each detected γ -rays using program Tv.
- (4) Computation of the number of decays for each γ ray using Eq. (6).
- (5) Computation of the average number of decays using Eq. (7).
- (6) Correction of the background coming from the vacuum chamber using Eq. (8).
- (7) Resolution of the Bateman equations to assess the fission rate τ using Eq. (9).
- (8) Correction of the correlation between E_k and q using Eq. (10).
- (9) Computation of the relative isotopic yield using Eq. (11).
- (10) Computation of the absolute isotopic yield using Eqs. (12) and (13).

Figure 2 shows the absolute isotopic yields for the mass $A = 139$ with the associated covariance matrix for two cases. On the left is shown the case using the actual uncertainties of I_γ , and on the right is shown the case using the uncertainty of the normalization intensity $I_{\text{norm}}^\gamma = 0$. In the latter, the total uncertainty is reduced by a factor of 4. The covariance

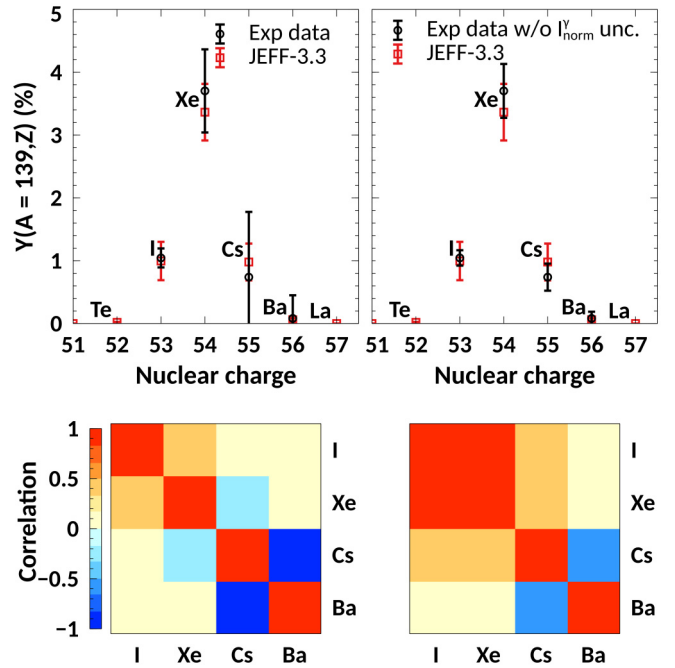


FIG. 2. Absolute isotopic yields for the mass $A = 139$ with all the uncertainties propagated (left) and for the case where $\Delta I_{\text{norm}}^\gamma = 0$ (right). A comparison with the JEFF-3.3 library is also displayed. Correlation matrices in both cases are also displayed (bottom).

matrix is also modified. In other words, the uncertainties are mainly coming from nuclear decay data. By improving these data, more accurate isotopic yields can be extracted. Finally, a comparison with the JEFF-3.3 database is also displayed and shows an overall good agreement. The experimental data were recorded in May 2013 [29] using a $7 \times 0.5 \text{ cm}^2$ target of $282 \mu\text{g cm}^{-2}$ of ^{241}Pu covered by a thin nickel foil ($\approx 0.25 \mu\text{m}$). This campaign was designed to measure isotopic yields for 8 masses. The derived local odd-even effect is $\delta_Z(A = 139) = 0.36 \pm 0.32$ in comparison with $\delta_Z^{\text{JEFF-3.3}}(A = 139) = 0.27 \pm 0.12$.

IV. FROM LOCAL ODD-EVEN EFFECT TO NEUTRON EMISSION USING FIFRELIN

In this work, the local odd-even effect $\delta_Z(A)$ as a function of the fission product kinetic energy for the mass $A = 139$ is computed. An experimental campaign in July 2016 [30] was carried out with a thinner target ($208 \mu\text{g cm}^{-2}$ of ^{241}Pu on $7 \times 0.5 \text{ cm}^2$) still covered by a thin nickel foil ($\approx 0.25 \mu\text{m}$). Here, all the steps described before are not necessary to extract the isotopic yields. For instance, it is counterproductive to correct $P(E_k)$, since an evolution of the fission product kinetic energy is investigated. The absolute normalization is also not necessary.

To interpret these results, a comparison with the Monte Carlo code FIFRELIN is performed. The aim is to test FIFRELIN assumptions. If an agreement is reached between the experimental data and FIFRELIN calculations, we can get feedback from the models used by FIFRELIN (the temperature ratio law for instance). However, energy loss corrections are needed to

go from the calculations (which directly reflect the fission process) to the experimental data. In the following part, details on the input data and the models used by FIFRELIN are presented. The energy loss correction process is also described. Finally, a sensitivity study on the main ingredients of the simulation will be shown.

A. FIFRELIN

Fission Fragment Evaporation Leading to an Investigation of Nuclear data (FIFRELIN) [31–33] is a Monte Carlo code developed at CEA Cadarache since 2010. Initially, the aim was to describe the deexcitation of fission fragments from their formation (after being fully accelerated) until they reach their ground state or a metastable state which then decay through β decay. Nowadays, the code can theoretically describe the deexcitation of any nucleus starting from a given nuclear level. FIFRELIN relies on preneutron nuclear data and models to compute the most accurate deexcitation path. The code can be split into two parts.

First, the fission process creates two fission fragments with a given mass, nuclear charge, kinetic energy, excitation energy, spin, and parity. Note that no complete set of experimental data exists for the reaction $^{241}\text{Pu}(n_{th}, f)$. Therefore, the preneutron isotopic yields $Y(A, Z)$ and total kinetic energy (TKE) yields $Y(\text{TKE}, A)$ are coming from the GEF code [34]. FIFRELIN samples the light fission fragment mass and nuclear charge using the $Y(A, Z)$ distribution. The total kinetic energy is then sampled using the $Y(\text{TKE}, A)$ distribution. The conservation laws allow one to assess the complementary heavy fragment characteristics (A, Z) and the associated kinetic energies (of both fragments). The repartition of the total excitation energy is mainly driven by a phenomenological temperature ratio law $R_T(A)$ with two free parameters RT_{\min} and RT_{\max} . By definition, there are three anchor points in the (A, R_T) space:

$$R_T(A_{\text{CN}}/2) = 1, \quad R_T(A_{\text{CN}} - 78) = RT_{\min}, \quad R_T(132) = RT_{\max}$$

with CN the compound nucleus. A linear interpolation is then made between each point. Finally the spin of each fission fragment is sampled from

$$P(J) \propto (2J + 1) \exp\left(-\frac{(J + 1/2)^2}{2\sigma^2}\right) \quad (14)$$

with σ^2 a free parameter for each fission fragment mass region (light and heavy). Those four free parameters are set using a target observable. Here, the target observable is the total average prompt neutron multiplicity $\bar{\nu} = 2.92$ [28]. The four parameters which reproduce this value are $RT_{\min} = 0.5$, $RT_{\max} = 1.2$, $\sigma_L = 7.2\hbar$, and $\sigma_H = 8.6\hbar$.

Second, both fission fragments will emit prompt (n, γ, e^-) particles until they reach a β decaying state. To do so, FIFRELIN completes the experimental nuclear level schemes coming from RIPL-3 database [35,36] by using nuclear level density (here the composite Gilbert and Cameron model [37]) and spin models (here the back-shifted Fermi gas model [35,36]). Once the nuclear level scheme is complete, the probability to go from a nuclear level i to a nuclear level j by emitting either n, γ , or e^- is

calculated within the notion of nuclear realization [33,38]. In this framework, different nuclear level schemes (for a given isotope) can be sampled, and for each sampled nuclear level scheme different deexcitation paths can be computed. For each emitted particle, different ingredients are used. The probabilities associated to the prompt neutron emission are calculated thanks to neutron transmission coefficients derived from an optical model (here the Koning-Delaroché model [39]). This optical model is used through the ECIS code [40]. The probabilities associated with the prompt γ emission are derived from the γ strength function (here, the enhanced generalized Lorentzian [41] model) and experimental information. The probabilities associated to the prompt e^- emission are calculated with the BRICC code [42] or come from experimental data.

FIFRELIN can compute the isotopic yields as a function of the fission product kinetic energy through an event-by-event analysis. However, the kinetic energy (after prompt neutron emission) computed by FIFRELIN needs to be corrected for the energy loss of fission products inside the target and its cover. To take it into account, FIFRELIN kinetic energy distributions are convoluted by a Landau distribution [43] which models the energy loss of ions through a thin layer [20,44]. Two free parameters are adjusted in order to reproduce the experimental kinetic energy distributions. Here, the energy loss is considered to be identical for each isotope of a given mass. Also, the parameters are adjusted for each BU point since the target and cover thickness may evolve over time (self-sputtering, oxidation of Ni foil, diffusion into backing [16]). Therefore, the mass $A = 136$ is used to fix the free parameters (see top plot in Fig. 3). Then, these fixed parameters are used to correct the kinetic energy distributions for $A = 139$ (see bottom plot in Fig. 3).

The comparison of experimental data and FIFRELIN of the local odd-even effect is shown in Fig. 4. The experimental point from the May 2013 campaign was added in order to show the reproducibility of the local odd-even effect using the LOHENGRIN spectrometer. In the following, only experimental data from July 2016 will be presented. Although FIFRELIN seems to overestimate the local odd-even effect, the same trend as in the experimental data can be observed. Finally, it is difficult to conclude on the agreement between FIFRELIN and the experimental data due to the large experimental uncertainties.

Therefore, a more precise and discriminant observable is needed to better estimate the difference between FIFRELIN calculations and the experimental data. The relative isotopic cumulative yields \mathcal{N}_c integrated over a period of time of $\Delta t_m = 30$ minutes fit these specifications:

$$\begin{aligned} \mathcal{N}_c(A, Z, E_k^\times, \Delta t_m) &= \sum_q \frac{N_d(A, q, E_k^\times, \Delta t_m, t)}{\text{BU}(t)}, \\ P_c(A, Z, E_k^\times, \Delta t_m) &= \frac{\mathcal{N}_c(A, Z, E_k^\times, \Delta t_m)}{\sum_Z \mathcal{N}_c(A, Z, E_k^\times, \Delta t_m)}, \end{aligned} \quad (15)$$

with P_c the relative isotopic cumulative yield probability. To compare simulations with P_c , the Bateman equation resolution \mathbf{B}^{-1} is applied to simulated data. Figure 5 shows the

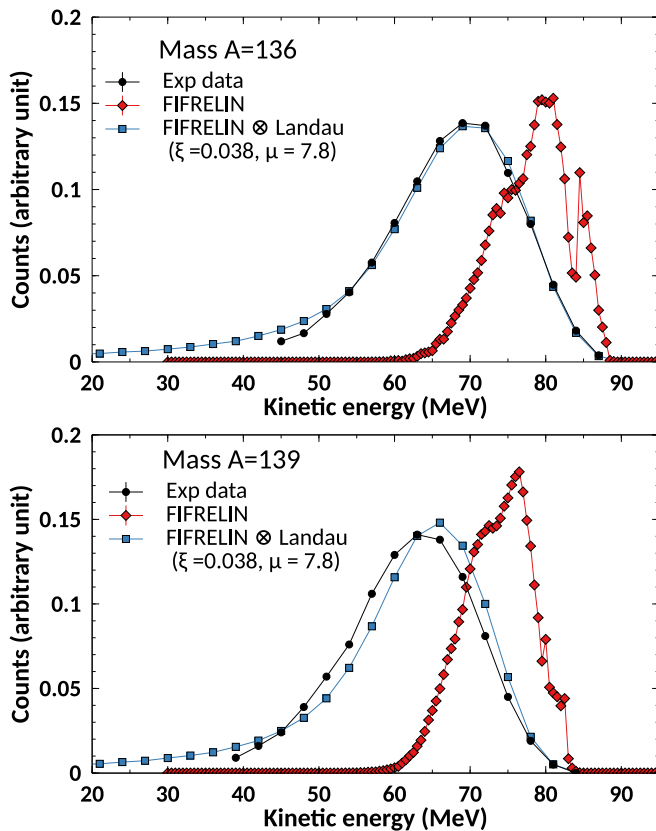


FIG. 3. Comparison between experimental kinetic energy distribution (black circle) and FIFRELIN calculation (red points). An agreement is reached by convoluting FIFRELIN with the Landau distribution. Parameters were fixed thanks to the mass $A = 136$ (top) and applied to mass $A = 139$ (bottom). The lines are to guide the eye. The experimental kinetic energy refers to the LOHENGRIN selected energy, i.e., after the cover foil.

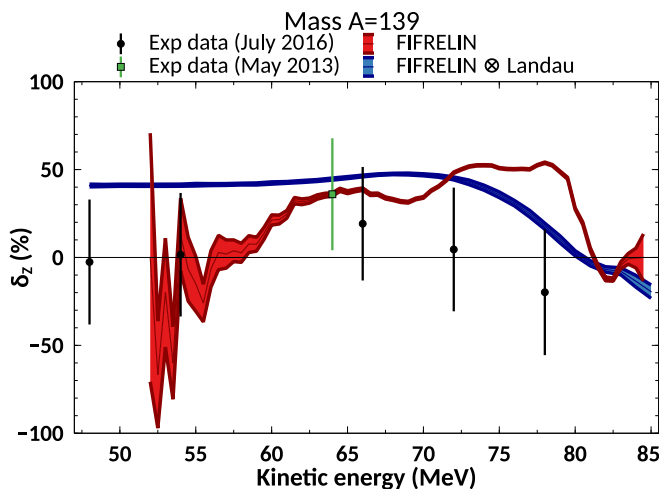


FIG. 4. Comparison between experimental data from the July 2016 campaign (black points) and from the May 2013 campaign (green point) and FIFRELIN calculations with (blue curve) and without (red curve) energy loss corrections. The experimental kinetic energy refers to the LOHENGRIN selected energy, i.e., after the cover foil.

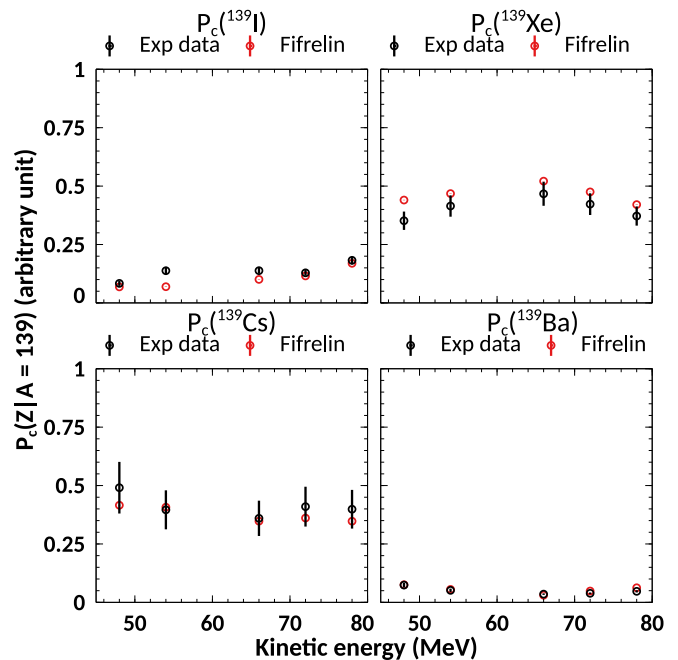


FIG. 5. Relative cumulated isotopic yield probability for experimental data (black points) and FIFRELIN calculations after energy loss corrections (red points). The experimental kinetic energy refers to the LOHENGRIN selected energy, i.e., after the cover foil.

results of such a comparison. The agreement between the experimental data and FIFRELIN is satisfactory even if a slight overestimation of FIFRELIN for Xe is observed. Indeed, all the experimental data (except the 54 MeV point for I) are compatible with FIFRELIN with a confidence level of 90%. In other words, FIFRELIN is validated in regards to the kinetic energy dependence of the mass $A = 139$.

B. Test of the model assumption

The next step is to look at the local odd-even effect as a function of the fission product kinetic energy computed by FIFRELIN without any energy loss correction. Figure 6 shows $\delta_z(A)$ as a function of the fission product kinetic energy (top) and the excitation energy (before neutron emission) (bottom). The different color points represent the $\delta_z(A)$ for fission events with different emitted neutrons. The results show that the structure of the $\delta_z(A)$ depends on the number of emitted neutrons.

It must be reminded that the adjusted parameters of FIFRELIN were fixed according to the average total prompt neutron emission $\bar{\nu}$ and not by using the relative cumulative yields of the mass $A = 139$. Therefore, the predictive power of FIFRELIN can be tested with these new experimental data. The good agreement between FIFRELIN and the experimental data indicates that the underlying hypotheses used in FIFRELIN are satisfactory. According to Fig. 6, $\delta_z(A)$ is driven by the neutron emission process. The neutron emission probability as a function of the excitation energy shows a steplike function, which can be interpreted as the average neutron energy separation to emit 1, 2, ... neutrons. In FIFRELIN, this process

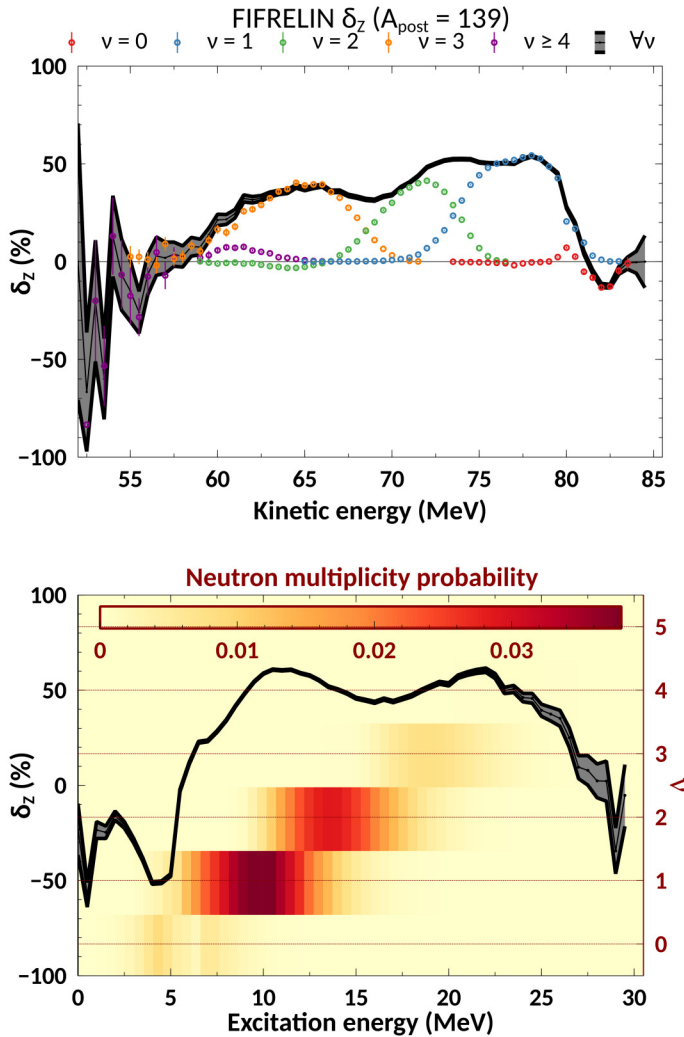


FIG. 6. Top: Local odd-even effect as a function of the fission product kinetic energy for different numbers of emitted neutrons: 0, 1, 2, 3, and ≥ 4 (displayed in colors). Bottom: Local odd-even effect as a function of the excitation energy before neutron emission (y axis on the left). Local odd-even effect as a function of the number of emitted neutrons (y axis on the right). The associated probabilities are displayed in colors (z axis on the top). No energy loss correction is taken into account.

is mainly due to the temperature ratio law and the neutron transmission coefficients.

A sensitivity analysis can be applied to two main ingredients of this analysis. The first one is the total excitation energy, which can be assessed through the temperature ratio law. To test the influence of the excitation energy on the local odd-even effect, a shift of ± 0.1 on the parameter RT_{\min} (which corresponds to a shift of ± 2 MeV in excitation energy) is performed. Figure 7 shows the impact of such a shift on the local odd-even effect and on the relative cumulative isotopic yield probability. Relative quantities (to the reference FIFRELIN calculation) are plotted. It shows that the temperature ratio law modification changes the parity at higher kinetic energy only. Nevertheless, the measurements are not accurate enough to provide a new constraint on this temperature ratio law. It

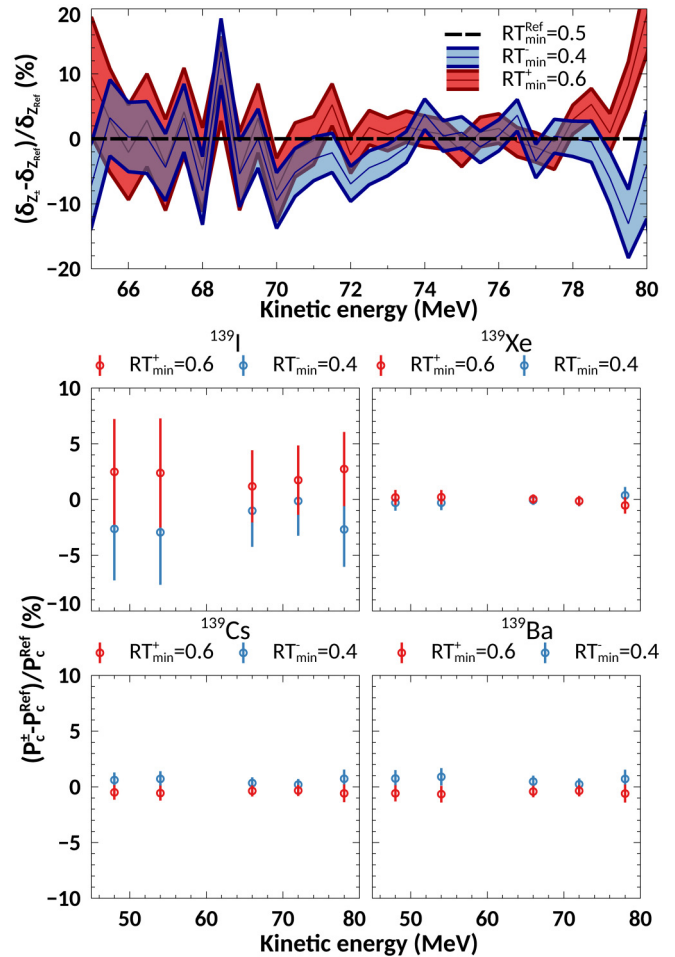


FIG. 7. Top: Local odd-even effect compared with the reference FIFRELIN calculation after a 0.1 shift on the parameter RT_{\min} (with $RT_{\min}^{\text{ref}} = 0.5$). A slight difference can be seen at higher kinetic energy. Bottom: Relative cumulated isotopic yield probability compared with the reference FIFRELIN calculation. No significant difference is observed (bottom). All calculations are corrected from the energy loss through the target and the cover foil.

can be explained by the impact of the energy loss through the target. With a thinner target, it should be possible to enhance the differences between the previous cases. Nonetheless, these results give confidence in the models and the processes used by FIFRELIN.

The second important ingredient is the preneutron isotopic yields. The aim is to test the reliability of these yields coming from GEF. To do so, the mean nuclear charge is shifted by ± 1 unit. In these cases, simulations are not in agreement with the experimental data anymore, as shown in Fig. 8. Therefore, the experimental data can also be used to validate the preneutron isotopic yields.

In conclusion, the experimental data can be seen as a local test for the mean neutron emission and the associated neutron probabilities within a restricted preneutron mass region (here $A = 139\text{--}143$).

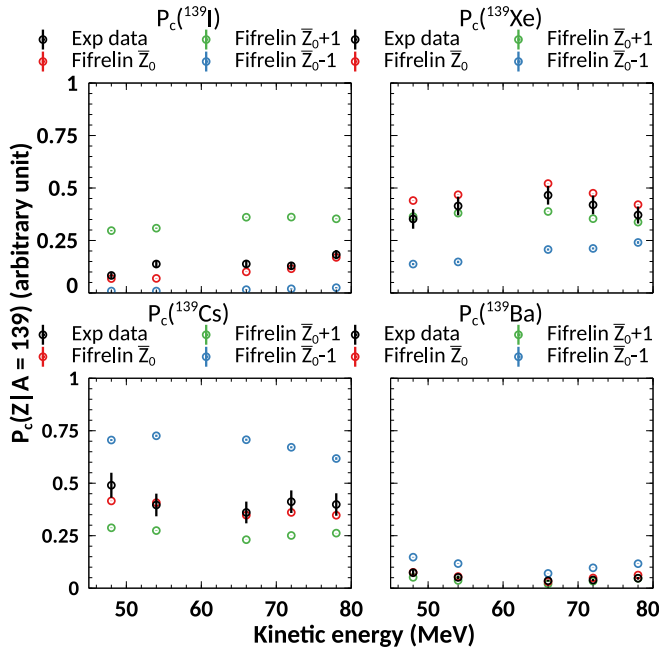


FIG. 8. Impact of one unit shift of the preneutron mean nuclear charge for all masses. A large impact is observed. The experimental kinetic energy refers to the LOHENGRIN selected energy, i.e., after the cover foil and the calculations are corrected from the energy loss through the target and the cover foil.

V. CONCLUSION AND OUTLOOK

The complete data analysis was presented and illustrated for the specific case of isobaric chain $A = 139$. Then, the local odd-even effect $\delta_Z(A)$ as a function of the fission product kinetic energy was assessed through measurements using the LOHENGRIN recoil spectrometer. Comparisons with the Monte Carlo code FIFRELIN were performed in order to interpret these experimental data in regards to the neutron emission process. The good match between the experimental results and the calculations coming from FIFRELIN indicates that the underlying models used are well chosen in the case of a fission event involving the mass $A = 139$. A sensitivity analysis shows these measurements are a probe to the local prompt neutron emission through all the deexcitation path assumptions used in FIFRELIN. However, the experimental data are not discriminant enough to highlight the impact of the initial excitation energy because of the energy loss inside the target. New measurements on a specific mass region (around $A = 132$) may give more constraints on the initial excitation energy and the temperature ratio law. These studies are complementary to the studies of the isomeric ratios evolution as a function of the fission product kinetic energy [11] or the studies of the correlation between the prompt γ cascade in coincidence with fission fragment and neutron observables [45–47].

ACKNOWLEDGMENTS

This work was supported by IN2P3, by the University of Grenoble Alpes, by the CEA project “SINET” and by “le défi

NEEDS.” The authors are grateful for the support of ILL and all the staff involved from CEA-Cadarache and LPSC.

APPENDIX A: RESOLUTION OF BATEMAN EQUATIONS

In this Appendix, we detail the way to go from the number of decays N_d of an isotope to the fission rate τ .

1. With a source term τ

The activities of a decay chain are ruled by the Bateman equation:

$$\begin{aligned} \frac{dN_0(t)}{dt} &= -\lambda_0 N_0(t) + \tau_0, \\ \frac{dN_1(t)}{dt} &= -\lambda_1 N_1(t) + \tau_1 + \text{BR}_{0 \rightarrow 1} \lambda_0 N_0(t), \\ &\vdots \\ \frac{dN_n(t)}{dt} &= -\lambda_n N_n(t) + \tau_n + \sum_{i=0}^{n-1} \text{BR}_{i \rightarrow n} \lambda_i N_i(t), \end{aligned} \quad (\text{A1})$$

with $N_{i=0,n}$ the population of the i th nucleus, $\lambda_{i=0,n}$ its decay probability, $\tau_{i=0,n}$ the associated fission source term and $\text{BR}_{i \rightarrow j}$ the probability of decaying from the nucleus i to the nucleus j . This equation can be written in a matrix form:

$$\frac{dN(t)}{dt} = \mathbf{BLN}(t) + \mathbf{T} = \mathbf{AN}(t) + \mathbf{T} \quad (\text{A2})$$

with

$$\begin{aligned} \mathbf{N} &= \begin{bmatrix} N_0 \\ \vdots \\ N_n \end{bmatrix}, \quad \mathbf{T} = \begin{bmatrix} \tau_0 \\ \vdots \\ \tau_n \end{bmatrix}, \quad \mathbf{L} = \begin{bmatrix} \lambda_0 & & 0 \\ & \ddots & \\ 0 & & \lambda_n \end{bmatrix}, \\ \mathbf{B} &= \begin{bmatrix} -1 & & 0 \\ & \ddots & \\ \text{BR}_{i \rightarrow j} & & -1 \end{bmatrix}. \end{aligned}$$

For each isotope i of the decay chain, the detected γ transition N_i^γ , during the measuring time Δt_m is written

$$\begin{aligned} \forall i, N_i^\gamma(\Delta t_m) &= I_\gamma \epsilon_\gamma f_\gamma \int_0^{\Delta t_m} \lambda_i N_i(t) dt \\ \Leftrightarrow \frac{N_i^\gamma}{I_\gamma \epsilon_\gamma f_\gamma} &= \int_0^{\Delta t_m} \lambda_i N_i(t) dt = N_{d_i}(\Delta t_m) \end{aligned} \quad (\text{A3})$$

with I_γ , ϵ_γ , and f_γ the intensity, the detection efficiency and the sum effect correction factor respectively. If we define

$$\forall i, X_i(\Delta t_m) = \int_0^{\Delta t_m} N_i(t) dt, \quad (\text{A4})$$

then

$$N_d(t) = \mathbf{LX}(t) \quad (\text{A5})$$

Since the functions used are \mathcal{C}^1 class, we can integrate and switch the derivative and the integration of Eq. (A2):

$$\frac{dX(t)}{dt} = \mathbf{AX}(t) + \mathbf{tT}. \quad (\text{A6})$$

To make $N_d(t)$ appear, we need to multiply Eq. (A6) by L and define $S = LAL^{-1}$:

$$\frac{dN_d(t)}{dt} = SN_d(t) + tLT. \quad (\text{A7})$$

Here S is an inferior triangle matrix; we can then diagonalize it: $S = RDR^{-1}$. If we define $Y(t) = R^{-1}N_d(t)$ and $C = R^{-1}LT$ and multiply Eq. (A7) by R^{-1} , it reads

$$\frac{dY(t)}{dt} = DY(t) + tC. \quad (\text{A8})$$

Since D is diagonal, we have n equations:

$$\forall i, \frac{dY_i(t)}{dt} = D_{ii}Y_i(t) + tC_i. \quad (\text{A9})$$

This is simply a first-order differential equation with time dependent tC_i second member. With the bounding condition $Y_i(t=0) = 0$ (which means that there was no nucleus at time 0), C_i is written

$$\forall i, C_i = \frac{D_{ii}^2}{e^{D_{ii}t} - 1 - D_{ii}t} Y_i(t) = E_{ii}(t) Y_i(t). \quad (\text{A10})$$

Finally,

$$T = BN_d(t) \quad \text{with} \quad B = L^{-1}RE(t)R^{-1}$$

$$\text{and the diagonal matrix } E(t) = \frac{D^2}{e^{Dt} - 1 - Dt}. \quad (\text{A11})$$

2. Without a source term

Moreover, in the case of the background correction, the Bateman equation to resolve is

$$\frac{dN(t)}{dt} = AN(t) \quad (\text{A12})$$

When integrating within a time t , we have

$$\frac{dX(t)}{dt} = AX(t) + M \Leftrightarrow \frac{dN_d(t)}{dt} = SN_d(t) + LM \quad (\text{A13})$$

with M the unknown which is related to the initial number of the nucleus. At the end, we have

$$M = BN_d(t) \quad \text{with} \quad B = L^{-1}RE(t)R^{-1}$$

$$\text{and the diagonal matrix } E(t) = \frac{D}{e^{Dt} - 1}. \quad (\text{A14})$$

3. Analysis method and background correction

For the background correction, an additional step must be performed in order to assess the parameter $N_{d\text{cont}}$ which reflects the contribution of vacuum residual background on a new measurement. Figure 1 shows the origin of the background. In the time interval $t = [t_0, t_1]$ the background coming from the vacuum chamber is recorded, $N_{d\text{bkg}}(t_1)$, and it allows one to determine M . We suppose that there is no initial background [$N_d(t=t_0) = 0$], then $N_{d\text{bkg}}(t=t_0) = 0$:

$$N_{d\text{bkg}}(t_1) = \frac{N_i^\gamma(t_1)}{I_\gamma \epsilon_\gamma f_\gamma}. \quad (\text{A15})$$

The contribution from the background during the measurement in the time interval $t = [t_2, t_3]$ is

$$N_{d\text{cont}} = \int_{t_2}^{t_3} LN(t)dt = N_d(t_3) - N_d(t_2). \quad (\text{A16})$$

From Eqs. (A5) and (A14), Eq. (A16) is written

$$\begin{aligned} N_{d\text{cont}} &= [B^{-1}(t_3) - B^{-1}(t_2)]M, \\ N_{d\text{cont}} &= [B^{-1}(t_3) - B^{-1}(t_2)]B(t_1)N_{d\text{bkg}}(t_1), \\ N_{d\text{cont}} &= R[E^{-1}(t_3) - E^{-1}(t_2)]E(t_1)R^{-1}N_{d\text{bkg}}(t_1) \\ \Leftrightarrow N_{d\text{cont}} &= R\left(\frac{e^{Dt_3} - e^{Dt_2}}{e^{Dt_1} - 1}\right)R^{-1}N_{d\text{bkg}}(t_1). \end{aligned} \quad (\text{A17})$$

APPENDIX B: GLOSSARY

This section summarizes all the notations used in the analysis part of the article.

A : mass of the nucleus A_ZX

Z : nuclear charge of the nucleus A_ZX

$\delta_Z(A)$: local odd-even effect

q : ionic charge

q_i : ionic charge for which kinetic energy distributions are performed

E_k : kinetic energy

ΔE_k : kinetic energy resolution

E_k^\times : kinetic energy for which ionic charge distributions are performed

\overline{E}_k : mean kinetic energy extracted from the kinetic energy distribution

σ_{E_k} : standard deviation extracted from the kinetic energy distribution

t : time when the measurement is made since the beginning of the experimental campaign

Δt_m : measuring time

BU(t) (burn-up): constructed observable in order to follow the loss of fissile material from the target as a function of time

$N(A, q, E_k, \Delta t_m, t)$: number of counts extracted from the ionization chamber

$\mathcal{N}(A, q_i)$: relative mass yield calculated from the kinetic energy distribution measured with the ionic charge q_i

$P(q)$: ionic charge probability derived from the ionic charge distribution

$\text{Cov}(\mathcal{N}(A, q_i), \mathcal{N}(A, q_j))$: element of the covariance matrix between the relative mass yield calculated from the kinetic energy distributions measured at q_i and q_j

$\overline{\mathcal{N}}(A)$: average relative mass yield

$Y(A)$: absolute mass yield

ϵ_γ : detection efficiency for a given γ transition

I_γ : absolute intensity for a given γ transition

I_γ^{rel} : relative intensity for a given γ transition

I_{norm}^γ : normalization factor for γ intensity

f_γ : sum effect correction factor for a given γ transition

$N_\gamma(A, Z, q, E_k^\times, \Delta t_m, t)$: number of counts extracted from the γ detectors for a given γ transition

$N_{d_\gamma}(A, Z, q, E_k^\times, \Delta t_m, t)$: number of decays derived from a given γ transition
 $\overline{N}_d(A, Z, q, E_k^\times, \Delta t_m, t)$: average number of decays
 $\text{Cov}(N_{d_{\gamma_i}}, N_{d_{\gamma_j}})$: element of the covariance matrix between the number of decays derived from the γ transition γ_i and the gamma transition γ_j
 $\overline{N}_{d_{\text{bkg}}}(A, Z, q, E_k^\times, \Delta t_m, t)$: average number of decays measured during the background measurement
 $\overline{N}_{d_{\text{cont}}}(A, Z, q, E_k^\times, \Delta t_m, t)$: average number of decays contaminating the current measurement
 $\overline{N}_{d_f}(A, Z, q, E_k^\times, \Delta t_m, t)$: average corrected number of decays

\mathbf{B} : matrix related to the Bateman equation resolution
 $\tau(A, Z, q, E_k^\times, t)$: fission rate
 $P(E_k^\times)$: probability to have the fission product at the selected kinetic energy E_k^\times
 $\mathcal{N}(A, Z)$: relative independent isotopic yield
 $\mathcal{N}_c(A, Z, E_k^\times, \Delta t_m)$: relative cumulative isotopic yield for a given kinetic energy
 $P_c(A, Z, E_k^\times, \Delta t_m)$: relative cumulative isotopic yield probability for a given kinetic energy
 k_{139} : normalization factor linking relative to absolute isotopic yield using the mass $A = 139$
 $Y(A, Z)$: absolute isotopic yield

- [1] O. Hahn and F. Strassmann, *Naturwissenschaften* **27**, 11 (1939).
 [2] L. Meitner and O. R. Frisch, *Nature (London)* **143**, 239 (1939).
 [3] H. Goutte, J. F. Berger, P. Casoli, and D. Gogny, *Phys. Rev. C* **71**, 024316 (2005).
 [4] P. Möller, A. J. Sierk, and A. Iwamoto, *Phys. Rev. Lett.* **92**, 072501 (2004).
 [5] J. Randrup and P. Möller, *Phys. Rev. Lett.* **106**, 132503 (2011).
 [6] E. Torleif, *Adv. Phys.* **9**, 425 (1960).
 [7] P. Fong, *Phys. Rev.* **102**, 434 (1956).
 [8] B. D. Wilkins, E. P. Steinberg, and R. R. Chasman, *Phys. Rev. C* **14**, 1832 (1976).
 [9] J. R. Nix and W. J. Swiatecki, *Nucl. Phys.* **71**, 1 (1965).
 [10] Y. Aritomo, S. Chiba, and F. Iwamoto, *Phys. Rev. C* **90**, 054609 (2014).
 [11] A. Chebboubi, G. Kessedjian, O. Litaize, O. Serot, H. Faust, D. Bernard, A. Blanc, U. Köster, O. Méplan, P. Mutti, and C. Sage, *Phys. Lett. B* **775**, 190 (2017).
 [12] J. Kaufmann, W. Mollenkopf, F. Gönnerwein, P. Geltenbort, and A. Oed, *Z. Phys. A* **341**, 319 (1992).
 [13] U. Quade, K. Rudolph, S. Skorka, P. Armbruster, H.-G. Clerc, W. Lang, M. Mutterer, C. Schmitt, J. Theobald, F. Gönnerwein, J. Pannicke, H. Schrader, G. Siegert, and D. Engelhardt, *Nucl. Phys. A* **487**, 1 (1988).
 [14] N. Boucheneb, P. Geltenbort, M. Asghar, G. Barreau, T. Doan, F. Gönnerwein, B. Leroux, A. Oed, and A. Sicre, *Nucl. Phys. A* **502**, 261 (1989).
 [15] P. Armbruster, M. Asghar, J. P. Bocquet, R. Decker, H. Ewald, J. Greif, E. Moll, B. Pfeiffer, H. Schrader, F. Schussler, G. Siegert, and H. Wollnik, *Nucl. Instrum. Methods* **139**, 213 (1976).
 [16] U. Köster, H. Faust, T. Materna, and L. Mathieu, *Nucl. Instrum. Methods A* **613**, 363 (2010).
 [17] G. Fioni, H. R. Faust, M. Gross, M. Hesse, P. Armbruster, F. Gönnerwein, and G. Münzenberg, *Nucl. Instrum. Methods A* **332**, 175 (1993).
 [18] F. Martin, Etude des distributions en masse, charge nucléaire et énergie cinétique des produits de fission de l'233U(nth,f) et du 241Pu(nth,f) mesurées auprès du spectromètre de masse Lohengrin (ILL), Ph.D. thesis, Université de Grenoble, 2013, <https://tel.archives-ouvertes.fr/tel-01288258/document>.
 [19] A. Chebboubi, Contribution à l'étude de la fission nucléaire: de LOHENGRIN à FIPPS, Ph.D. thesis, Université Grenoble Alpes, 2015, <https://tel.archives-ouvertes.fr/tel-01272599/document>.
 [20] S. Julien-Laferrrière, Approche expérimentale et phénoménologique des rendements de la fission induite par neutron thermique du 239Pu et du 241Pu, Ph.D. thesis, Université Grenoble Alpes, 2018, <https://tel.archives-ouvertes.fr/tel-01995046/document>.
 [21] S. Julien-Laferrrière, A. Chebboubi, G. Kessedjian, and O. Serot, *EPJ Nucl. Sci. Technol.* **4**, 25 (2018).
 [22] Y. K. Gupta, D. C. Biswas, O. Serot, D. Bernard, O. Litaize, S. Julien-Laferrrière, A. Chebboubi, G. Kessedjian, C. Sage, A. Blanc, H. Faust, U. Köster, A. Ebran, L. Mathieu, A. Letourneau, T. Materna, and S. Panebianco, *Phys. Rev. C* **96**, 014608 (2017).
 [23] A. Chebboubi, S. Julien-Laferrrière, J. Nicholson, G. Kessedjian, O. Serot, A. Blanc, D. Bernard, H. Faust, Y. Kim, U. Köster, A. Letourneau, O. Litaize, O. Méplan, P. Mutti, M. Rapala, M. Ramdhane, and C. Sage, EPJ Web Conf. (to be published).
 [24] J. Theuerkauf, S. Esser, S. Krink, M. Luig, N. Nicolay, O. Stuch, and H. Wolters, *Program Tv* (Institute for Nuclear Physics, Cologne, 1993).
 [25] Y. Khazov, A. A. Rodionov, S. Sakharov, and B. Singh, *Nucl. Data Sheets* **104**, 497 (2005).
 [26] S. Sudár, TrueCoinc - A program for calculation of true coincidence correction for gamma rays, Tech. Rep. No. IAEA-TECDOC-1275 (Institute of Experimental Physics, Debrecen, 2009), pp. 37–48.
 [27] M. Chadwick, M. Herman, P. Obložinský, M. Dunn, Y. Danon, A. Kahler, D. Smith, B. Pritychenko, G. Arbanas, R. Arcilla, R. Brewer, D. Brown, R. Capote, A. Carlson, Y. Cho, H. Derrien, K. Guber, G. Hale, S. Hoblit, S. Holloway, T. Johnson, T. Kawano, B. Kiedrowski, H. Kim, S. Kunieda, N. Larson, L. Leal, J. Lestone, R. Little, E. McCutchan, R. MacFarlane, M. MacInnes, C. Mattoon, R. McKnight, S. Mughabghab, G. Nobre, G. Palmiotti, A. Palumbo, M. Pigni, V. Pronyaev, R. Sayer, A. Sonzogni, N. Summers, P. Talou, I. Thompson, A. Trkov, R. Vogt, S. van der Marck, A. Wallner, M. White, D. Wiarda, and P. Young, *Nucl. Data Sheets* **112**, 2887 (2011).
 [28] A. Santamarina, D. Bernard, P. Blaise, M. Coste, A. Courcelle, T. Huynh, C. Jouanne, P. Leconte, O. Litaize, S. Mengelle, G. Noguère, J.-M. Ruggiéri, O. Serot, J. Tommasi, C. Vaglio, and J.-F. Vidal, The JEFF-3.1.1 Nuclear Data Library, Tech. JEFF Rep. No. 22 (NEA, Paris, 2009).
 [29] O. Serot, D. Bernard, S. Chabod, A. Chebboubi, H. Faust, G. Kessedjian, U. Köster, A. Letourneau, O. Litaize, F. Martin, T. Materna, O. Méplan, S. Panebianco, and C. Sage, Fission

- product yield measurements in the heavy mass region for the $^{241}\text{Pu}(\text{nth},\text{f})$ reaction, Institut Laue-Langevin (ILL) dataset, doi: [10.5291/ILL-DATA.3-01-596](https://doi.org/10.5291/ILL-DATA.3-01-596) (2013).
- [30] O. Litaize, C. Amouroux, D. Bernard, A. Blanc, A. Chebboubi, H. Faust, G. Kessedjian, U. Köster, A. Letourneau, T. Materna, O. Méplan, S. Panebianco, C. Sage, and O. Serot, Isotopic and isomeric yields measurement in the near symmetric mass region of the $^{241}\text{Pu}(\text{nth},\text{f})$ reaction, Institut Laue-Langevin (ILL) dataset, doi: [10.5291/ILL-DATA.3-01-624](https://doi.org/10.5291/ILL-DATA.3-01-624) (2016).
- [31] O. Litaize and O. Serot, *Phys. Rev. C* **82**, 054616 (2010).
- [32] O. Litaize, O. Serot, and L. Berge, *Eur. Phys. J. A* **51**, 177 (2015).
- [33] D. Regnier, O. Litaize, and O. Serot, *Comput. Phys. Commun.* **201**, 19 (2016).
- [34] K.-H. Schmidt, B. Jurado, C. Amouroux, and C. Schmitt, *Nucl. Data Sheets* **131**, 107 (2016).
- [35] R. Capote, M. Herman, P. Obložinský, P. Young, S. Goriely, T. Belgia, A. Ignatyuk, A. Koning, S. Hilaire, V. Plujko, M. Avrigeanu, O. Bersillon, M. Chadwick, T. Fukahori, Z. Ge, Y. Han, S. Kailas, J. Kopecky, V. Maslov, G. Reffo, M. Sin, E. Soukhovitskii, and P. Talou, *Nucl. Data Sheets* **110**, 3107 (2009).
- [36] M. Verpelli and R. Capote, International nuclear data committee, Update of RIPL nuclear levels segment, Tech. Rep. No. INDC(NDS)-0702 (IAEA, Vienna, 2015), <https://www-nds.iaea.org/publications/indc/indc-nds-0702/>.
- [37] A. Gilbert and A. G. W. Cameron, *Can. J. Phys.* **43**, 1446 (1965).
- [38] F. Bečvář, *Nucl. Instrum. Methods Phys. Res., Sect. A* **417**, 434 (1998).
- [39] A. Koning and J. Delaroche, *Nucl. Phys. A* **713**, 231 (2003).
- [40] J. Raynal, Notes on ECIS94, Tech. Rep. No. CEA-N-2772 (CEA, Saclay, 1994).
- [41] J. Kopecky and M. Uhl, *Phys. Rev. C* **41**, 1941 (1990).
- [42] T. Kibédi, T. Burrows, M. Trzhaskovskaya, P. Davidson, and C. Nestor, *Nucl. Instrum. Methods Phys. Res., Sect. A* **589**, 202 (2008).
- [43] L. Landau, in *Collected Papers of L. D. Landau* (Pergamon, Oxford, 1965).
- [44] A. Chebboubi, O. Serot, G. Kessedjian, O. Litaize, A. Blanc, D. Bernard, H. Faust, S. Julien-Laferrrière, U. Köster, A. Letourneau, T. Materna, O. Méplan, P. Mutti, M. Rapala, and C. Sage, *EPJ Web Conf.* **146**, 04063 (2017).
- [45] T. Wang, G. Li, L. Zhu, Q. Meng, L. Wang, H. Han, W. Zhang, H. Xia, L. Hou, R. Vogt, and J. Randrup, *Phys. Rev. C* **93**, 014606 (2016).
- [46] M. Jandel, B. Baramsai, T. Bredeweg, A. Couture, A. Favalli, A. Hayes, K. Ianakiev, M. Iliev, T. Kawano, S. Mosby, G. Rusev, I. Stetcu, P. Talou, J. Ullmann, D. Vieira, C. Walker, and J. Wilhelmy, *Nucl. Instrum. Methods Phys. Res., Sect. A* **882**, 105 (2018).
- [47] C. Michelagnoli, A. Blanc, E. Ruiz-Martinez, A. Chebboubi, H. Faust, E. Froidefond, G. Kessedjian, M. Jentschel, U. Köster, P. Mutti, and G. Simpson, *EPJ Web Conf.* **193**, 04009 (2018).